Applied Physics A (2024) 130:322
https://doi.org/10.1007/s00339-024-07458-y

Applied Physics A
Materials Science & Processing

Studies on the structural, thermal and luminescence properties of $Sr_{1-x}ZrSi_2O_7$:xEu^{3+} phosphors for solid state lighting

Manorama Sahu[1,2] · **Ishwar Prasad Sahu**[3]

Received: 21 December 2023 / Accepted: 16 March 2024 / Published online: 18 April 2024

Abstract

This paper reports the synthesis, structural, thermal and luminescence properties of $Sr_{1-x}ZrSi_2O_7$:xEu^{3+} ($x = 0.01 \le x \le 0.05$ mol) phosphors by solid-state reaction method in air. The optimal Eu^{3+} ion concentration in $Sr_{1-x}ZrSi_2O_7$:xEu^{3+} phosphor is 0.04 mol. The monoclinic crystal structure with P21/c space group was confirmed by the powder X-ray diffractometry (PXRD) technique. Thermal behavior of the present phosphors was investigated which shows better characteristics. Under 396 nm excitation, Eu^{3+} ions activated $Sr_{1-x}ZrSi_2O_7$ phosphors exhibited a strong red emission centered at 617 nm due to the f–f transition of $^5D_0 \rightarrow {}^7F_2$ transition. The critical doping concentration of Eu^{3+} ion was $x = 0.04$ mol and the critical distance was determined as 19.1117 Å. The energy transfer among Eu^{3+} ions in $Sr_{1-x}ZrSi_2O_7$ phosphors was found to be a dipole–dipole interaction. Consequently, optimal phosphor shows a thermal stability up to 420 K, superior to that in analogous reports. And the quantum efficiency of prepared $Sr_{1-x}ZrSi_2O_7$:xEu^{3+} phosphor with 396 nm excitation was calculated to be nearly 72%. The photometric results indicate that the synthesized Orange-Red phosphor can be potentially applicable for solid-state lighting and display devices applications.

Keywords $Sr_{1-x}ZrSi_2O_7$:xEu^{3+} · Thermal stability · Critical distance · Photometric properties · Solid-state lighting

1 Introduction

In the last decades, phosphors have become key importance of technological development. Many devices have lighting units that are made by LED [1]. This LED has a basic principle of phosphors that are adjuvant with the luminescent properties of the rare earth (RE) ions doped in the selected host materials [2]. Thus, the type of RE ions and features of the host materials are the main attention during the development of phosphor materials. Due to its vast range of possible applications in solid-state lighting, full-colour display systems and white light-emitting diodes (WLEDs) recently gained great attraction. The phosphor-converted light-emitting diode (pc-LED) technology is a renowned solid-state lighting method [3].

The host lattice and the sort of doped ion has a crystal structure which is recognized to have a substantial influence on the luminescence properties of phosphors [4]. Phosphors with a silicate host are the most useful luminescent material, with several advantages like inexpensive cost, higher luminous efficiency, and a simple production technique. Furthermore, RE doped silicates are known for their charge stability, high thermal stability, and low sintering temperatures, all of which have sparked interest [5]. Zirconium silicates construct an essential class due to their magnificent optical properties associated with photothermal stability and low thermal conductivity. furthermore, zirconia possess low phonon energy and it has been catchy for use as support for RE ions, since the transition possibilities are increased, creating this material fascinating for different applications. [6]. Some zirconium silicate phosphors are reported as the potential for white LEDs application such as $CaZrSi_2O_7$:Eu^{3+} [7]; $BaZrSi_3O_9$:Eu^{3+} [8]; and $Ca_2ZrSi_4O_{12}$:Eu^{3+} [9] have been proved as a good luminescence material to exhibit excellent optical properties.

✉ Ishwar Prasad Sahu
ishwarprasad1986@gmail.com

[1] Department of Physics, Government Polytechnic, Kabirdham 491995, Chhattisgarh, India

[2] Department of Applied Physics, Shri Shankaracharya Institute of Professional Management and Technology, Raipur 492015, Chhattisgarh, India

[3] Department of Physics, Indira Gandhi National Tribal University, Amarkantak 484887, Madhya Pradesh, India

In this study, we have chosen strontium zirconium silicate [($SrZrSi_2O_7$)–SZSO] as a host matrix. A SZSO phosphor would be ideal from the manufacturing point of view, because the raw materials are abundant and are relatively inexpensive. The SZSO crystal was first time reported by Huntelaar et al. [10] and then Blasse et al. [11] and other researchers subsequently studied the ultraviolet (UV) photoluminescence (PL) of SZSO. The luminescent emission color of phosphor usually depends on types of doped RE ions, which are highly affected by the host [12, 13]. The arrangement of host can affect the crystal field environment of RE ions, bringing about the energy level transition change of RE ions [14–16]. As the activators commonly used of trivalent rare-earth (RE^{3+}) ions due to their advantages of narrow emission band in visible range based on the inherent transition properties, resultant high efficiency and high lumen obtain. It is distinguished that Eu^{3+} is a excellent dopant and has a superior emission spectrum in reddish region [17–20]. Thus, it is essential to choose a good host material to synthesize orange–red phosphor used for white LEDs excited by Near Ultra–Violet (NUV).

To the best of our knowledge, before this work $Sr_{1-x}ZrSi_2O_7$:xEu^{3+} (S_{1-x}ZSO:xEu) phosphor has not been reported, therefore, in this research work, structural, thermal and PL properties of S_{1-x}ZSO:xEu phosphors have been prepare by solid state reaction method. The luminescence characteristics of the discussed phosphor according to the change in the concentration and effect of the activator ions has been studied. In addition, we also explored the photometric properties [Commission Internationale Eclairage (CIE), Color rendering index (CRI), Color Correlated Temperature (CCT), Color Purity (CP) and Quantum Efficiency (QE)] of the discussed materials. The prepared Eu^{3+} doped SZSO phosphors to explore orange–red emitting phosphor that may be applicable for solid-state lighting and display devices.

2 Experimental

2.1 Materials preparation

The $Sr_{1-x}ZrSi_2O_7$:xEu^{3+} ($x = 0.01 \le x \le 0.05$ mol) were prepared in air by the solid-state reaction technique using high temperature programmable furnace. The highly pure oxides of $SrCO_3$, ZrO_2, SiO_2, H_3BO_3 and Eu_2O_3 with proper stoichiometric proportions was weighted to the normal composition, and agate mortar and pestle were used for grinding the mixture thoroughly; pre-heated at 1000 °C for 1 h and then heated at 1450 °C for 4 h in Al_2O_3 crucibles. A small quantity of H_3BO_3 was added as flux. After completion of the process of sintering, the temperature of programmable furnace is cooled down to room temperature. The synthesized phosphors were ground to obtain fine powder. The sample code of synthesized powder products has tabulated in Table 1. The chemical reaction used for stoichiometric calculation is:

$$SrCO_3 + ZrO_2 + 2SiO_2 \rightarrow SrZrSi_2O_7 + CO_2 \quad (1)$$

$$2SrCO_3(1-x) + 2ZrO_2 + 4SiO_2 + x2Eu_2O_3 \rightarrow 2Sr_{1-x}ZrSi_2O_7 : xEu^{3+} + 2CO_2 + 3O_2 \quad (2)$$

2.2 Measurement techniques

The PXRD experiments were performed using a Bruker D8-Advance XRD (operated in 40 kV and 20 mA) diffractometer with CuKα radiation in the 2θ range of 10–80° in steps of 0.02. The PXRD patterns obtained were then compared with the standard JCPDS files no. 82–1206. Rietveld refinement was performed by using Full Prof software. In the calculations made, a pseudo-voigt type shape of the peaks was adopted and the graphical interface Win PLOTR. For the analysis of thermal behavior, TGA/ DSC have been carried out separately using TGA2/DSC3 by METTLER TOLEDO, respectively. A baseline was measured with an empty crucible after that the well mixed reactants are placed at alumina crucible. In each measurement approx ~ 0.05 g and ~ 0.5 g of prepared materials were used for DSC and TGA, respectively. The powders were heated under nitrogen gas (70 mL/min) from 40 to 1500 °C with heating rate of 20 K/min. The FESEM (FE-SEM, XL30, Philips) was used for imaging of surface morphology of the prepared sample and the elemental (qualitative and quantitative) analysis was also investigated by the Energy Dispersive X-Ray Spectroscopy (EDS). The combination, composition, purity, vibrational properties and other impurity of all of the functional and finger print groups of synthesized compounds was observed by FTIR, Alpha-II ECO ATR, BRUKER. The PL spectra of the prepared powders are recorded by using a spectrofluorometer Shimadzu (RF 5301-PC). Decay curve was measured by fluoro

Table 1 Sample code of synthesized Sample

S. no	Sample code	Synthesized Sample
1	SZSO	$SrZrSi_2O_7$
2	SZSO:0.01Eu	$Sr_{0.99}ZrSi_2O_7$: $0.01Eu^{3+}$
3	SZSO:0.02Eu	$Sr_{0.98}ZrSi_2O_7$: $0.02Eu^{3+}$
4	SZSO:0.03Eu	$Sr_{0.97}ZrSi_2O_7$: $0.03Eu^{3+}$
5	SZSO:0.04Eu	$Sr_{0.96}ZrSi_2O_7$: $0.04Eu^{3+}$
6	SZSO:0.05Eu	$Sr_{0.95}ZrSi_2O_7$: $0.05Eu^{3+}$
7	$S_{1-x}ZSO_xEu$	$Sr_{1-x}ZrSi_2O_7$:xEu^{3+} ($x = 0.01 \le x \le 0.05$ mol)

max-4cp_1715D-2218-FM equipped with a 150 W ozone free Xenon arc lamp as the excitation light source. PL emission spectra of the materials were converted into the CIE 1931 color coordinate system and color coordinates corresponding to the prominent emission were determined.

3 Results and discussion

3.1 XRD analysis

In this study, the crystallinity, crystallite size, micro-strain, dislocation density, and crystal structure of PXRD result were analyzed. The typical PXRD plot of SZSO and S_{1-x}ZSO:*x*Eu samples are shown in Fig. 1, it is well matched with standard JCPDS:82–1206 file [21] and comparatively it is observed that monoclinic phase and the space group is P21/c (14) with $Z=4$ present in the synthesized samples which is showing that doping of Eu^{3+} ions does not create any remarkable change in the host crystal structure. Because of valuable ionic radius (r_2) of Eu^{3+} ions [$r_2=1.21$ Å coordination number (CN) = 8, $r_2=1.09$ Å (CN) = 6] should replace Sr^{2+} [$r_1=1.332$ Å (CN) = 9, $r_1=1.274$ Å (CN) = 8, $r_1=1.224$ Å (CN) = 7, $r_1=1.128$ Å (CN) = 6] rather than Zr^{4+} [$r=0.98$ Å (CN) = 8, $r=0.86$ Å (CN) = 6, $r=0.73$ Å (CN) = 4] and Si^{4+} [$r=0.40$ Å (CN) = 6, $r=0.26$ Å (CN) = 4] [22, 23]. In the SZSO host lattice, a similar ionic radius and the same valance state predict the Eu^{3+} ions will occupy the Sr^{2+} sites according to Eq. (2) [24, 25]. No any extra diffraction peaks were found in the diffraction pattern of the samples and it is indicating that no extra impurities were present in the single phase synthesized materials [23].

$$Dr = 100 * \frac{r1(CN) - r2(CN)}{r1(CN)} \tag{3}$$

where, $r_{1(CN)}$ = the radius of the host cations, $r_{2\,(CN)}$ = radius of doped ion, and $D_{r\,=}$ radius percentage difference. If the radius difference between host cations and doped ion exceeded than 30%, then new compound will produce. In our case; using Eq. (3), it is found that $Dr=5.0235\%$ [8 (CN)] and 3.3687% [6 (CN)], it should be $D_r<15\%$. It indicates that the doping of Eu^{3+} ions have no influence on the crystal structure of the SZSO system [25, 26]. When divalent Sr^{2+} ions are substituted by trivalent Eu^{3+} ions, various defects can be induced due to the charge compensation mechanism. In order to keep charge balance is that two Eu^{3+} ions can put back three Sr^{2+} ions to stabilize the charge of these phosphors, therefore generate two positive defects ($Eu^{\cdot}_{Sr}$), each having one positive charge and one V''_{Sr} negative defect (Eq. (4)). The vacancy defect (V''_{Sr}) acts as a donor and the defects ($2Eu^{\cdot}_{Sr}$) as an acceptor of the electrons. This process can be expressed by the Kroger – Vink notations.

$$2Eu^{3+} + 3Sr^{2+} \rightarrow 2Eu^{\cdot}_{Sr} + V''_{Sr} \tag{4}$$

$$V''_{Sr} \rightarrow V^{*}_{Sr} + 2e^{-}$$

$$2Eu^{\cdot}_{Sr} + 2e^{-} \rightarrow 2Eu^{*}_{Sr}$$

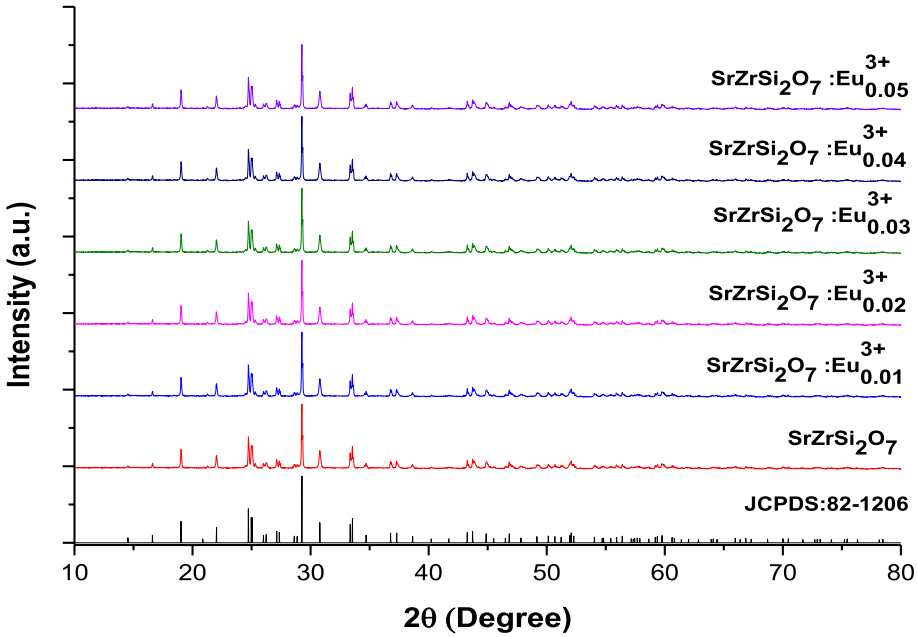

Fig. 1 PXRD patterns of SZSO and S_{1-x}ZSO:xEu phosphors with different concentration and JCPDS file

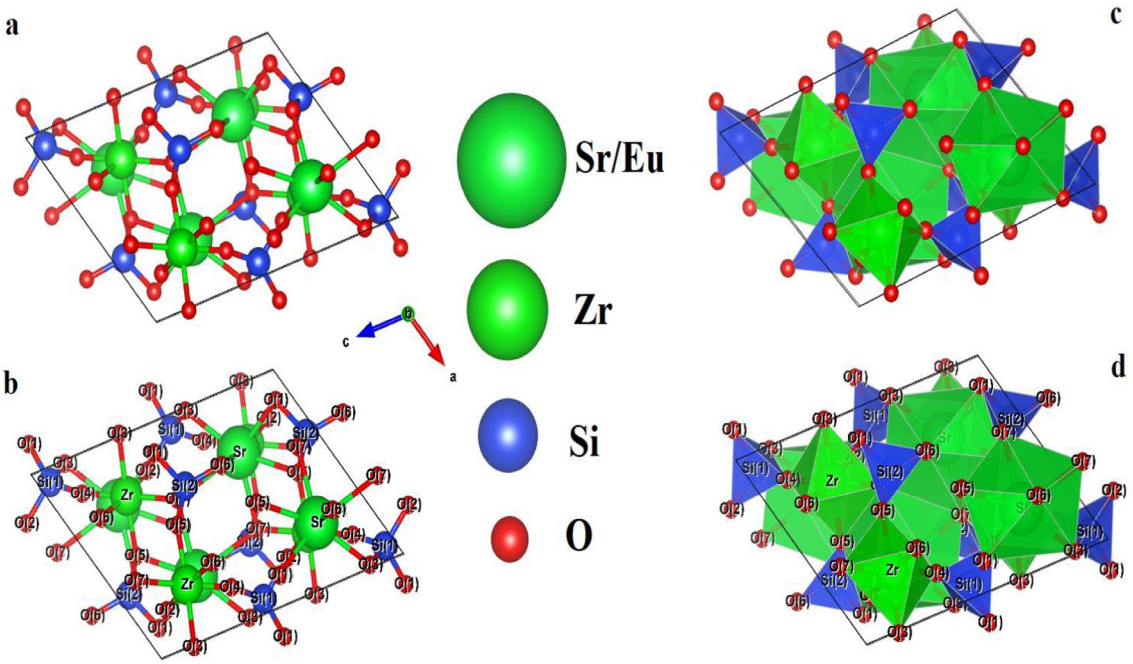

Fig. 2 Crystal structure for SZSO and $S_{1-x}ZSO{:}xEu$ phosphors

Figure 2 shows the 3D crystal structure of SZSO and $S_{1-x}ZSO_xEu$ phosphors can be described using VESTA software. The three-dimension crystal framework of SZSO is constructed by alternating layers of corner-sharing [ZrO_6] octahedron and of [Si_2O_7] groups formed from slightly distorted [SiO_4] tetrahedron sharing one common oxygen (O) atom and being arranged in nearly eclipsed conformation, and strontium (Sr) atom is coordinated by 8 O atom to form a distorted [SrO_8] dodecahedron [10, 27, 28]. The lattice parameters of the optimum SZSO:0.04Eu phosphor was calculated using Rietveld refinement software and compared with the $SrZrSi_2O_7$ Crystallographic Information File (CIF): 2,009,819. The refined values of SZSO:0.04 E has monoclinic structure are well matched with the standard lattice parameters and as shown in Table 2.

The crystal structure of the compound SZSO:0.04Eu was determined using Rietveld refinement of PXRD data. The Eu^{3+} was assumed to substitute the site for Sr^{2+} ion [7]. Figure 3 displayed the observed, calculated and difference PXRD patterns of prepared SZSO:0.04Eu phosphors. According to the CIF (ID: 2009819) standard host matrix (pure SZSO) was found to be $a = 7.76170$ Å, $b = 8.07130$ Å, $c = 10.05590$ Å, $V = 584.510867$ Å^3 while $\alpha = 90.000°$, $\beta = 111.9000°$, $\gamma = 90.000°$ and $Z = 4$. Table 1 represents the Rietveld refinement analysis of the prepared SZSO:0.04Eu phosphor, and the result of the fit obtained was reflected in terms of χ^2, R_P, R_{wp}, WR_P, R_{exp} etc. has slightly increased from that the standard host lattice [29]. There is slightly augmentation of lattice parameters due to Eu^{3+} incorporation into the SZSO lattice. Reason behind was the ionic radii of Eu^{3+} is lower than Sr^{2+} and its easily replaceable, causing decrease in unit cell parameters. Alternatively, the decrease in crystal density is ascribed to decreasing cell volume [30]. The detailed comparison among the crystallographic data of SZSO:0.04Eu phosphor with CIF of SZSO refinement parameters are summarized in Table 2. Position of SZSO atoms along with their respective occupancies is listed in Table 3.

Crystallite (grain) sizes were estimated through PXRD pattern using Debye Scherer formula (Eq. (5)) and Micro-crystal strain was calculated by the Williamson–Hall (W–H) plot (Eq. (6) and (7)). Figure 4 displayed the Micro-strain plot of SZSO with $S_{1-x}ZSO{:}xEu$ phosphors of different concentration. The broadening of the peak in the prepared sample grows not only due to crystallite size but also ascribed to be extant strain [31]. The dislocation density was also calculated using (Eq. (8)).

$$< Ds \geq \frac{k\lambda}{\beta cos\theta} \tag{5}$$

$$\beta\cos(\theta) = \frac{k\lambda}{D} + \varepsilon\sin(\theta) \tag{6}$$

Table 2 Rietveld refinement Crystallographic data of SZSO:0.04Eu phosphor

S. no.	Refinement parameters	Refinement Values of $Sr_{0.96}ZrSi_2O_7$:0.04Eu^{3+} Phosphor	$SrZrSi_2O_7$ As per CIF File: 2009819
1	Empirical Formula	$Sr_{0.96}ZrSi_2O_7$: 0.04Eu^{3+}	$SrZrSi_2O_7$
2	Formula weight	347.011	347.011
3	Crystal System	Monoclinic	Monoclinic
4	Space group:	P 21/c	P 21/c
5	Laue Class:	2/m	–
6	Unit Cell Parameters	$a=7.76061$ Å, $b=8.07063$ Å, $c=10.05507$ Å, $\alpha=90.000°$, $\beta=111.87489°$, $\gamma=90.000°$	$a=7.76170$ Å, $b=8.07130$ Å, $c=10.05590$ Å, $\alpha=90.000°$, $\beta=111.9000°$, $\gamma=90.000°$
7	Vol:	584.508948 $Å^3$	584.510867 $Å^3$
8	Calculated density	4.402 g/cm^3	–
9	Z	4	4
10	R_p:	9.40	–
11	R_{wp}:	13.0	–
12	R_{exp}:	6.53	–
13	Chi(χ^2):	2.35	–
15	R_{Bragg}-factor:	6.8	–
15	RF-factor	4.73	–
16	$D_{W\text{-}Stat.}$:	0.5947	–
17	GoF Index	0.093	–
18	$D_{W\text{-}exp}$	1.8986	–

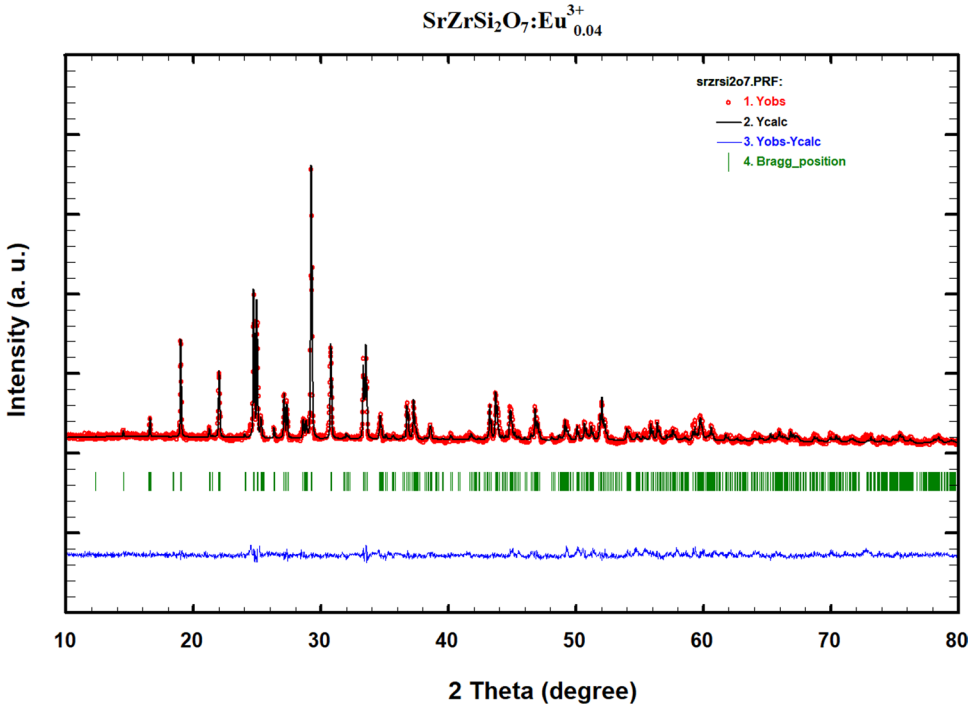

Fig. 3 Rietveld refinement plot of SZSO:0.04Eu phosphor

Table 3 Comparison of refinement crystallographic data for atomic parameters of SZSO and SZSO:0.04Eu phosphor

S. no	Atom	Valence state	Atomic co-ordinate						B_{iso}		Occupancy/sof		Mult
			x		y		z						
			Host	Doped	Host	Doped	Host	Doped	Host	Doped	Host	Doped	
1	Sr	+2	0.28250	0.28849	0.48170	0.48533	0.29450	0.29356	1.000	2.561	1.000	1.044	4
2	Zr	+4	0.25970	0.25999	0.01100	0.01097	0.24600	0.23921	1.000	− 0.101	1.000	0.974	4
3	Si	+4	0.06500	0.07664	0.24840	0.22035	0.45770	0.45656	1.000	2.662	1.000	1.148	4
4	Si	+4	0.67370	0.70028	0.21360	0.22087	0.46050	0.47303	1.000	1.654	1.000	0.176	4
5	O	− 2	0.86750	0.85362	0.15390	0.17459	0.43900	0.41363	1.000	1.691	1.000	1.219	4
6	O	− 2	0.19180	0.19281	0.26890	0.27045	0.62500	0.64851	1.000	6.235	1.000	1.746	4
7	O	− 2	0.01150	0.01312	0.42140	0.42170	0.36950	0.35381	1.000	0.366	1.000	1.598	4
8	O	− 2	0.16980	0.19714	0.13440	0.13381	0.38090	0.40941	1.000	− 5.345	1.000	0.894	4
9	O	− 2	0.52570	0.50605	0.09150	0.05821	0.34920	0.48158	1.000	2.543	1.000	0.177	4
10	O	− 2	0.69430	0.65938	0.20500	0.19964	0.62390	0.54290	1.000	50.939	1.000	4.545	4
11	O	− 2	0.63310	0.60283	0.40440	0.37530	0.40640	0.34471	1.000	7.324	1.000	1.511	4

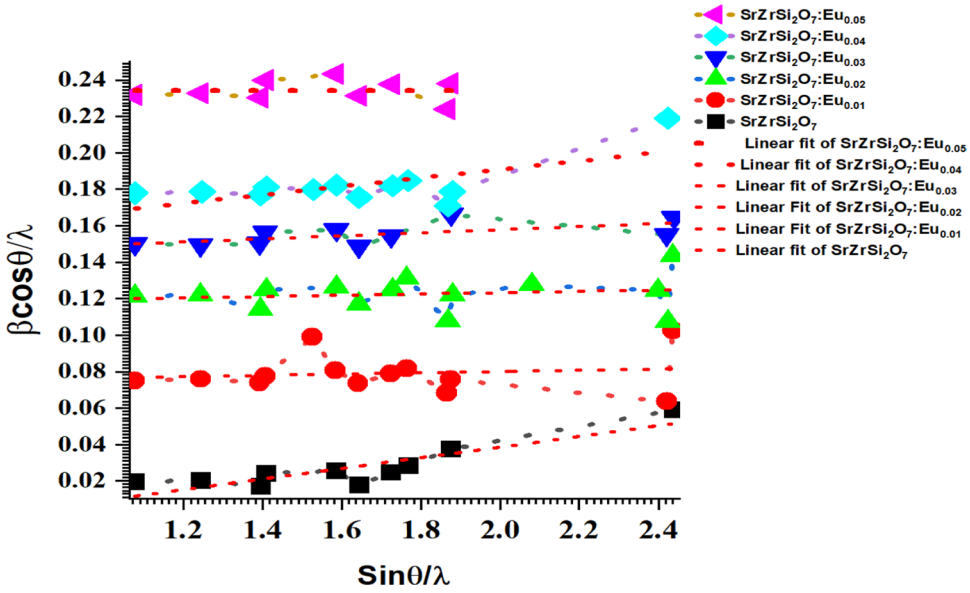

Fig. 4 Micro-strain plot of SZSO and S_{1-x}ZSO:*x*Eu phosphors of different concentration

Table 4 Calculated values of peak angles, FWHM, crystallite size, d-spacing, and micro strain of prepared S_{1-x}ZSO:xEu phosphors

Sample	2θ (degree)	β	D_s	δ	d	$D_{W\text{-}H}$	Micro strain ε
SZSO	29.34304	0.16284	50.43019600	0.0003932	0.304133283	53.83925903	0.000687356
SZSO:0.01Eu	29.29052	0.16958	48.42003000	0.0004265	0.304666655	51.68708963	0.000715892
SZSO:0.02Eu	29.34304	0.18976	43.27599661	0.0005339	0.405933811	46.20143835	0.000800987
SZSO:0.03Eu	29.34304	0.16290	50.41162134	0.0003934	0.304133283	58.18011444	0.000687609
SZSO:0.04Eu	29.34304	0.16045	51.18138433	0.0003817	0.480087255	54.64122743	0.480087255
SZSO:0.05Eu	29.34304	0.15417	53.26621986	0.0003524	4.558996573	62.01576628	0.000650760

$$\varepsilon = \frac{\beta cos\theta}{4} \tag{7}$$

Dislocation density (δ)

$$\delta = \frac{1}{D^2} \tag{8}$$

where $< D_s >$ is the mean crystallite size, λ is X-ray wavelength, β is full-width half maxima (FWHM), θ is the angle of diffraction, k is the shape factor ($k = 0.9$), ε = micro-strain and δ = dislocation density. The mean crystallite size of the sintered samples was calculated by the Debye Scherer formula and W–H plot, Micro-crystal strain with dislocation density were calculated and listed in Table 4.

3.2 TGA/DSC

A simultaneous TGA/DSC system is very useful for thermal profiling samples. TGA curve provides in detail mass loss of the sample in the desired temperature range while DSC curve pertain information about the heat flow to detect thermal events such as liquefy and crystallization, furthermore to provide specific and precise transition temperatures. The TGA/DSC curves of prepared SZSO:0.04Eu sample are displayed in Fig. 5. TGA/DSC curve for the prepared sample shows that the weight is decreases for TGA up to ~ 650 °C/DSC (~ 250 °C) than constant up for TGA up to ~ 1150 °C/DSC (~ 750 °C). A total weight loss of 0.5561% was observed in TGA curve. From DSC curve, a melting peak was observed for SZSO: 0.04 Eu phosphor, the melting temperature is observed at 1416.50 °C with a change in enthalpy of − 90 J/g. The weight loss of samples is due to removed carbon impurities and trapped of associated gasses [32, 33]. Hence, carbon dioxide gas must be released during one reaction. Considering the possible reaction between $SrCO_3$, ZrO_2, and SiO_2 (Eq. 2), we may be seeing the formation of SZSO and carbon dioxide is released in the form of gas.

3.3 Field emission scanning electron microscopy (FESEM)

The micrographs with different magnification of prepared SZSO:0.04Eu phosphor were also recorded through the use of FESEM in Fig. 6a–c. The surface of the SZSO:0.04Eu phosphor has shown irregular distribution of the crystallite sizes. As seen from the images, the discussed phosphors are in the form of microstructures and particles are generally in the shape of sphere [34]. The morphological images displays that the particles are accumulated tightly with each other. From the FESEM image, it can be noticed that the prepared sample are highly distinctive, more or less uniform, and compact grain distribution. Using the SEM

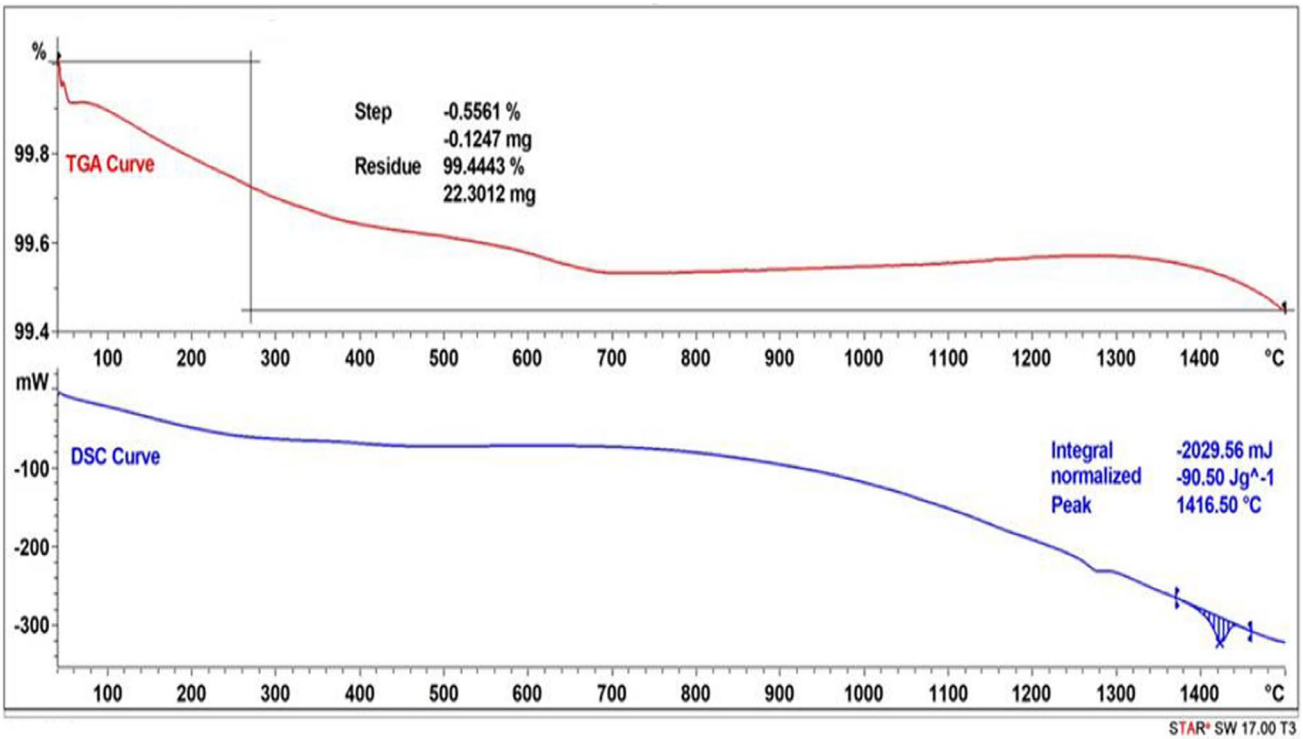

Fig. 5 TGA/DSC Curve of SZSO:0.04Eu phosphor

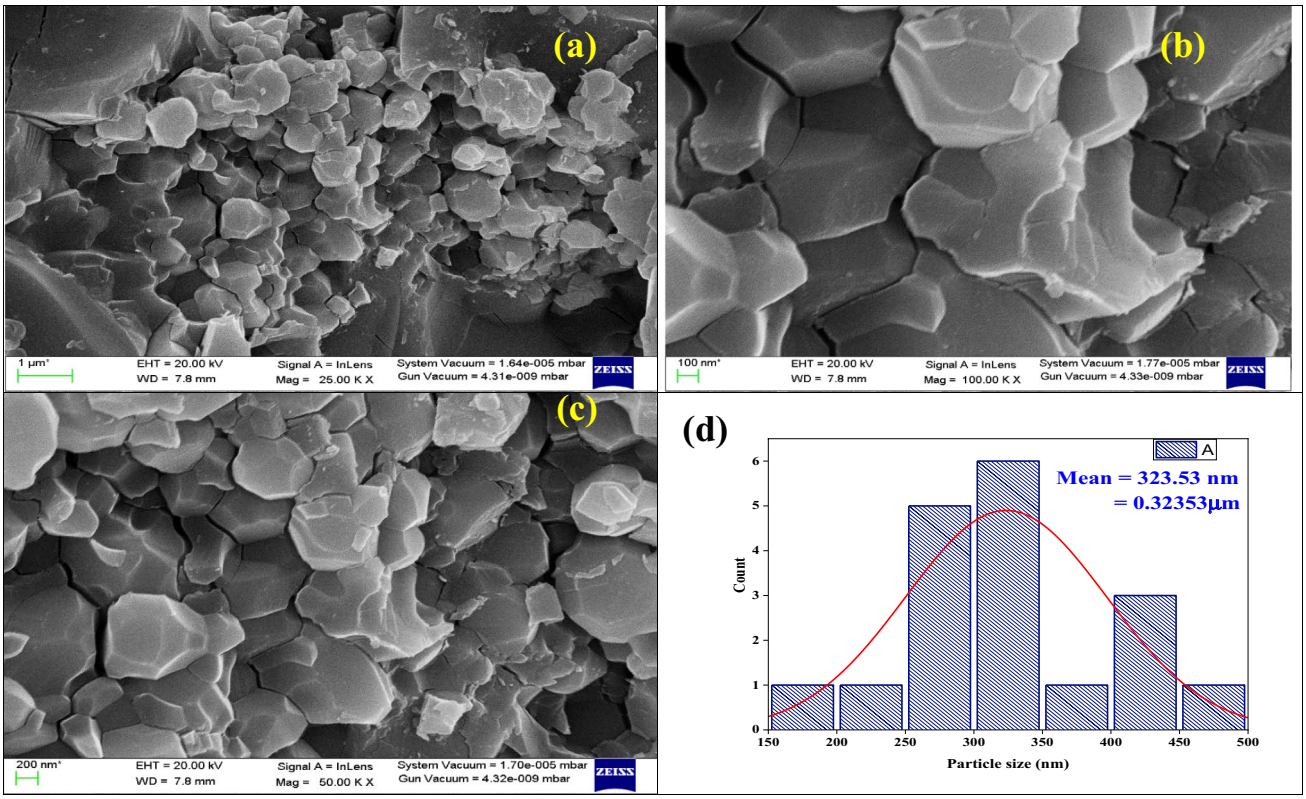

Fig. 6 **a**–**c** FESEM image and **d** Particle size distribution of SZSO:0.04Eu phosphor

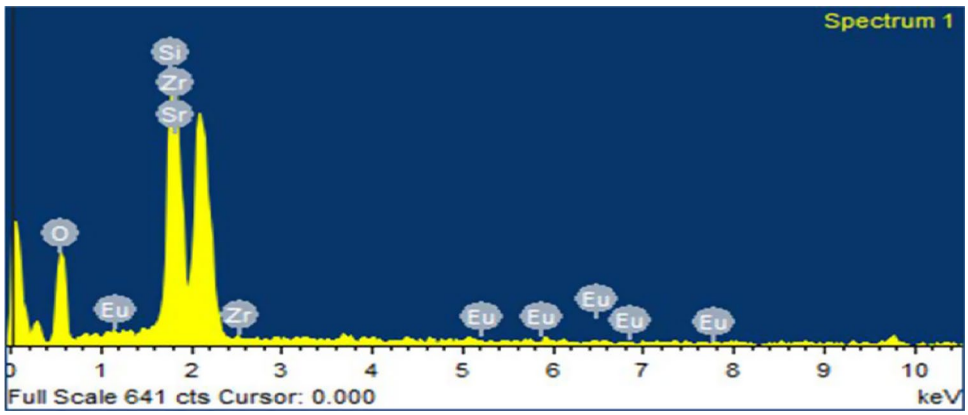

Fig. 7 EDS spectra of SZSO:0.04Eu phosphor

picture and the lineal interecept method (Heyn's method, Eq. (9)), the average particle size D_{SEM} is computed.

$$D_{SEM} = 1.56 \times \frac{L}{MN} \tag{9}$$

where, respectively, M, L, and N denote the picture's magn efication, the length of line drawn on the image, and the gr ain boundaries the line intersects. According to statistic, the mean size is around 0.32353 µm. Image J software was

Table 5 Chemical composition of SZSO:0.04Eu phosphor

S. no.	Standard	Elements	Atomic (%)	Weight (%)
1	SiO_2	O K	36.09	69.72
2	SiO_2	Si K	11.06	12.17
3	SrF_2	Sr L	17.08	6.03
4	Zr	Zr L	35.49	12.02
5	EuF_3	Eu L	0.28	0.06
Total			100	100

use to identify the mean particle size by the histogram, as shown in Fig. 6d.

3.4 Energy dispersive X-ray spectroscopy (EDS)

The EDS technique was used to identify elemental compositions of SZSO:0.04Eu phosphor is shown in Fig. 7. The different peaks of the spectrum revealed the elemental composition of strontium (Sr), zirconium (Zr), silicon (Si), oxygen (O), and europium (Eu) in the synthesized compound SZSO:0.04Eu phosphor. It is notified that no other peaks are obtained, that result is indicating homogeneity and purity of SZSO:0.04 phosphor. The elemental composition of discussed phosphor is listed in Table 5.

3.5 Fourier transform infrared (FTIR) spectra

Figure 8 shows the FTIR spectra of S_{1-x}ZSO:xEu phosphors. In the shown spectrum the absorption bands of zirconate and silicate groups were distinctly visible. In the 1400–500 cm^{-1} region several bands are typical metal oxygen absorptions Si-O_{nb}, Zr–O_2–Zr, Zr–O/ Sr–O, and Si–O–Si stretching

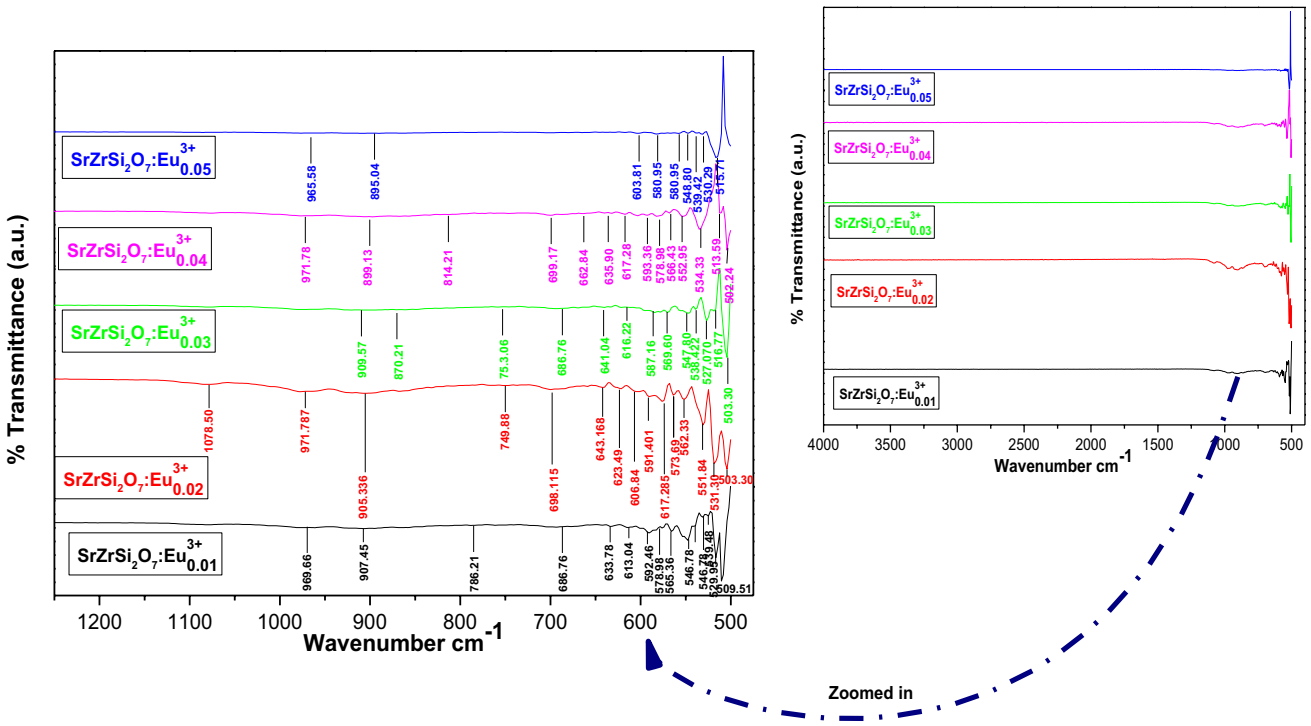

Fig. 8 FTIR Spectra of S_{1-x}ZSO:xEu phosphors

Table 6 FTIR assignment of S_{1-x}ZSO:xEu phosphors

S. no	Assignment	SZSO:0.01Eu	SZSO:0.02Eu	SZSO:0.03Eu	SZSO:0.04Eu	SZSO:0.05Eu	Type
1.	Si-O_{nb} (1100–700)	969.66, 907.45	1078.50, 971.78, 905.33, 749.88	909.57, 870.21, 753.06	971.78, 899.13, 814.21	965.58, 895.04	Asymmetrical stretch/Bending
2.	Zr-O_2-Zr (700–600)	786.21	698.11, 686.76, 643.16, 623.49, 606.84,	686.76, 641.04, 616.22	699.17, 662.84, 635.90	603.81	Vibrational Stretch
3.	Zr-O/Sr–O (600–550)	633.78, 613.04, 592.46, 565.36	591.40, 578.98, 573.69, 562.33, 551.84	587.16, 569.60	617.28, 593.36, 578.89, 566.43, 552.95	580.95, 560.21, 548.86, 530.29	Symmetric bonding
4.	Si–O-Si (550–500)	546.78, 539.48, 529.95, 509.51	531.30, 503.30	547.80, 538.42, 527.07, 516.77, 503.30	534.33, 513.59, 502.24	540.807, 539.42, 515.71	Anti-symmetric stretching

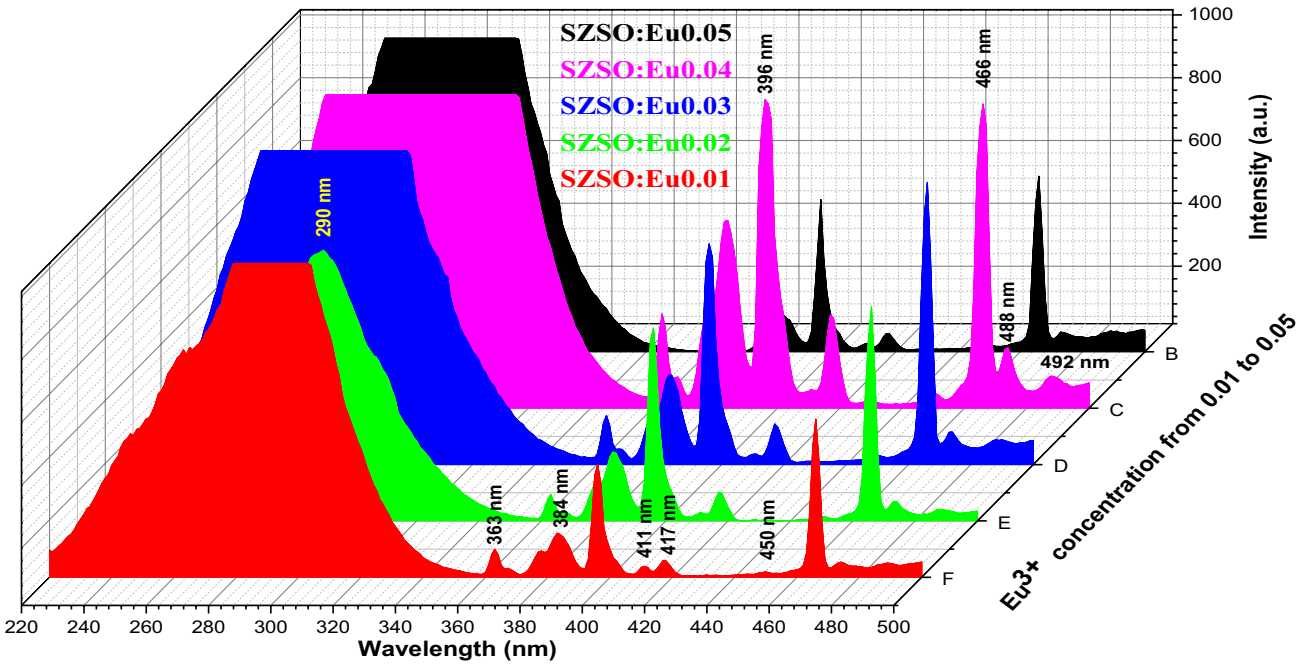

Fig. 9 Excitation spectra of S_{1-x}ZSO:*x*Eu phosphors of different concentration

frequencies were found [35]. The Si-O_{nb} asymmetrical stretch/bending for the silicate tetrahedral show infrared absorption bands, located at about ~ 1100–700 cm^{-1}. The vibrational stretch at ~ 700–600 cm^{-1} may be assigned the Zr–O_2–Zr symmetric and bending vibrations. The symmetric bonding of Zr–O/Si–O appeared at nearly ~ 600–550 cm^{-1}. The anti-symmetric stretching bands arounds ~ 550–400 cm^{-1} (in our case 550–500 cm^{-1}) are attributed due to the Si–O–Si vibrations [36, 37]. FTIR assignment of S_{1-x}ZSO:*x*Eu phosphors of different concentration were listed in the Table 6.

3.6 Photoluminescence (PL)

3.6.1 PL excitation spectra

Figure 9 shows the PL excitation (PLE) spectra of S_{1-x}ZSO:*x*Eu phosphors for varying concentrations monitored at 617 nm emission wavelength at room temperature. PL emission spectra were recorded from 220 to 500 nm range. Recorded PLE spectra has given broadband from 220 to 350 nm and it is centered at around 290 nm assigned to the $O^{2-} \rightarrow Zr^{4+}$ charge transfer (CT) and CT from oxygen 2p to an empty $4f^7$ orbitals of Eu^{3+} ion ($O^{2-} \rightarrow Eu^{3+}$). Other sharp peaks are obtained in the range of 360–500 nm due to the 4f → 4f transition of Eu^{3+} ions from the ground state of $^7F_0$ to its excitation levels [38, 39]]. The excitation peaks were found at 363 ($^7F_0 \rightarrow {}^5D_4$), 384 ($^7F_0 \rightarrow {}^5L_7$), 396 ($^7F_0 \rightarrow {}^5L_6$), 411 ($^7F_0 \rightarrow {}^5D_3$), 417 ($^7F_0 \rightarrow {}^5D_2$), 450, 466, 488 and 492 ($^7F_0 \rightarrow {}^5D_1$) nm are due to transition. [32, 33]. Among them, the strong excitation peaks are located at 396 nm. In the excitation spectra, it is observed that the intensity of CT band transition is weaker than the intra-f transition (~ 396 nm and 466 nm). This phenomenon of transition may be due to the weak covalency of the Eu^{3+} and O^{2-} in the S_{1-x}ZSO:*x*Eu phosphors [34, 35]. The optimum intensity of excitation spectra is obtained for 0.04 mol doping concentration. According to the results, the prepared phosphor may be efficient for excitation in NUV lights. The excitation wavelengths are well-matched with the common commercially available blue Indium Gallium Nitride (InGaN) chip which is very useful for application in a white light generation [40].

3.6.2 PL emission spectra

Figure 10 shows that PL emission spectra graph of prepared S_{1-x}ZSO:*x*Eu phosphors with different doping concentrations were monitored at 396 nm excitation wavelength. The emission spectra show five emission peaks at 581, 594, 617, 654 and 702 nm in agreement with $^5D_0 \rightarrow {}^7F_0$, $^5D_0 \rightarrow {}^7F_1$, $^5D_0 \rightarrow {}^7F_2$, $^5D_0 \rightarrow {}^7F_3$ and $^5D_0 \rightarrow {}^7F_4$ respectively. The strong emission peaks located at 594 nm ($^5D_0 \rightarrow {}^7F_1$) and 617 nm ($^5D_0 \rightarrow {}^7F_2$) in which the most intense peak obtained at 617 nm indicates that favorer in red color emission [27]]. The emission spectra of phosphors indicate similar profile is obtained for different doping concentrations which are shown in Fig. 10. The shape of all emission spectra is

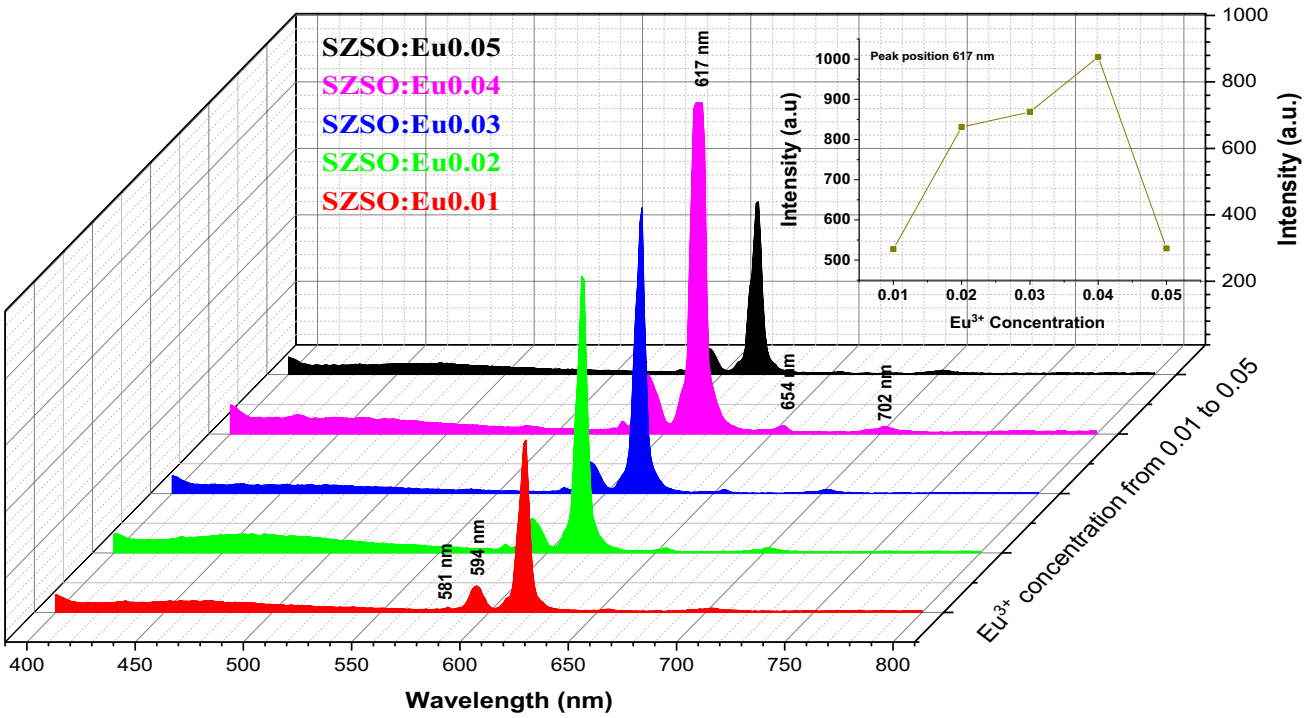

Fig. 10 Emission spectra of S_{1-x}ZSO:xEu phosphors of different concentration

similarly demonstrating that the host structure does not affect by the increasing doping concentration of Eu^{3+} ions [39]. In other words, the valance electron of Eu^{3+} ions are shielded by the outer electron 5 s and 5p orbitals, and hence the f –f transition of the Eu^{3+} ions are very small affected by ligand ions of the host lattice [40]. It is observed that the emission peaks are almost same for the 396 nm excitation wavelengths. Most of the f–f transition of the RE ions is very slightly affected by the environment of the host matrix. Some transitions are very sensitive to the environment of the host and become more intense than the other one, such type of transition is known as a hypersensitive transition [34].

From the emission spectra of synthesized sample $^5D_0 \rightarrow {}^7F_2$ transition is dominant over the $^5D_0 \rightarrow {}^7F_1$ transition, which indicates the transition $^5D_0 \rightarrow {}^7F_2$ is hypersensitive, Kanchan Mondal et al. [27] is already reported that the emission peak obtained at 594 nm ascribed to the magnetic dipole transition (MDT). The emission peaks at 617 nm and 702 nm are owing due to electric dipole transition (EDT). The peaks at 581 nm and 654 nm are become forbidden from both MDT and EDT [41, 42]. In the present case, the dominant EDT ($^5D_0 \rightarrow {}^7F_2$) indicates that the Eu^{3+} ions are located at non-inversion symmetry sites in the SZSO host lattice. Because when MDT are dominating then the Eu^{3+} ions are located at inversion symmetry sites, and while the EDT are dominating then Eu^{3+} ions are located at non-inversion symmetry sites in the host matrix

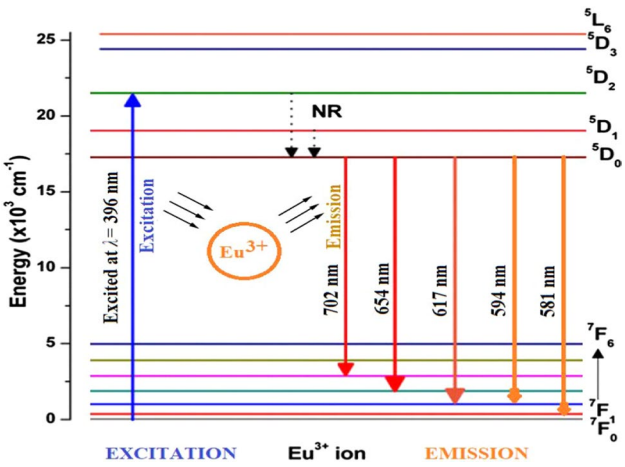

Fig. 11 Schematic Energy Level diagram of the S_{1-x}ZSO:xEu phosphors

[27]. Asymmetric Ratio (R/O) is calculated via emission intensity of the ($^5D_0 \rightarrow {}^7F_2$)/($^5D_0 \rightarrow {}^7F_1$) transition to identify site symmetry, covalent nature, and polarization of environment of Eu^{3+} ions in the host lattice. The R/O for optimum doping concentration is found to be around 1.6 for 396 nm for an excitation wavelength. R/O is greater than 1 is suggested that Eu^{3+} ions occupied a non-centro symmetric site which may be favorable to obtain of high color purity. The

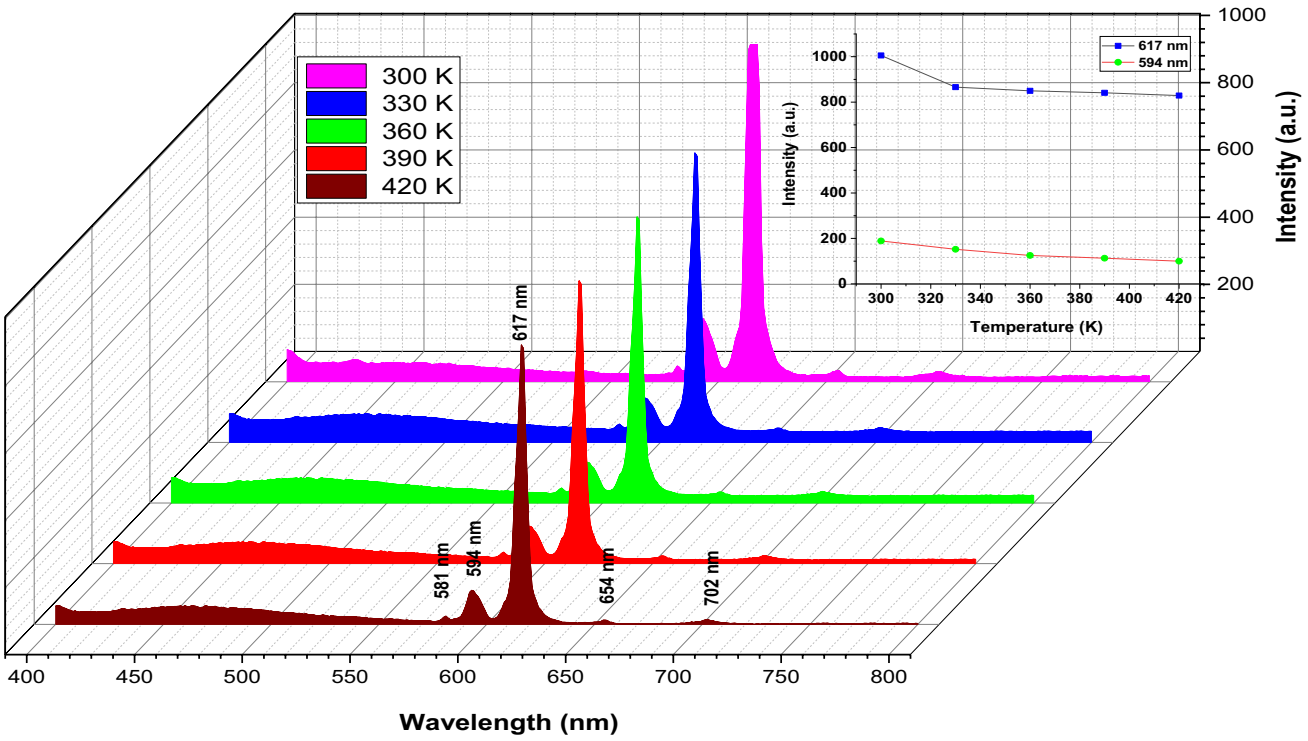

Fig. 12 Temperature dependent emission spectra of SZSO:0.04Eu phosphor

value of R/O is strongly depending on the occupation site of cation, bond nature, lattice distortion, and nature of the host material [41, 42].

Under the excitation at 396 nm, different transition possible in case of $S_{1-x}ZSO:xEu$ phosphors are illustrated in Fig. 11**.** Initially, the electrons excited from the ground state ($^7F_0$) to the higher excited level ($^5L_6$ and $^5D_2$) correspond to 396 nm and 466 nm excitation wavelength, respectively. The electron from that level gets to relax to the lowest excited level ($^5D_0$) via the non-radiative (NR) transitions. Then, electrons return back to the ground levels ($^7F_0$, $^7F_1$, $^7F_2$, $^7F_3$ and $^7F_4$) with radiative transitions. These different radiative transitions give different colors (orange, orange-red and red) with different intensities and overall give to the orange-red luminescence.

3.6.3 Temperature dependent emission spectra

Thermal stability is a major criterion in solid state lighting, particularly in WLEDs applications. Figure 12 shows the temperature dependent emission spectra of SZSO:0.04Eu phosphor was investigated at various temperatures in the range from room temperature to nearly 420 K. It is evident that the shapes and peak positions of the spectra remain unchanged when the temperature was increased [43]. For the comparison point of view, the excitation wavelength was fixed at 396 nm, which can effectively emit many sharp lines in the emission spectra ranging from 581 to 702 nm. With the increasing temperature, the intensity of the transition originated from $^5D_0 \rightarrow {}^7F_j$ ($J = 0, 1, 2, 3, 4$) transition as expected. It is observed that with increasing temperature the peak intensity of the prepared material decreases gradually Fig. 12 (inset). The progressive decrease in PL intensity is due to the augmented non-radiative transition. It can also be noted that with increasing temperature the peak wavelength of discussed phosphor remains constant, thus the thermal stability was ensured [30].

When the Eu^{3+} concentration is increased up to the 0.04 mol simultaneously emission intensity is also increases and optimum intensity were obtained for 0.04 mol. After then further Eu^{3+} concentration increases emission intensity is decreased due to the concentration quenching (CQ). The CQ graph is shown in Fig. 10 (inset). It is prominent that when the doping concentration of Eu^{3+} has increased, the distance between the Eu^{3+} ions become miniature which amplified non-radiative energy transfers between neighboring Eu^{3+} ions [31]. The energy transfer mechanism originated from, radiation re-absorption, exchange interaction or multipolar interaction which depends on the value of critical distance (R_c) which is calculated using the Blasse formula [43] shown in Eq. (10).

$$R_c \approx 2\left[\frac{3V}{4\pi X_c Z}\right]^{\frac{1}{3}} \quad (10)$$

Where X_c is the critical concentration of the dopant ion, Z is the number of cation sites in SZSO, and V is the volume of the unit cell. In the present case, the experimental and analytic values of $V = 584.508948$ (Å)^3, $Z = 4$ and $X_c = 0.04$ mol respectively. Calculations are made to determine the value of R_c is 19.1117 Å. It is well known that when the Rc < 5 Å, Exchange interactions are usually predominant. In our case, $R_c > 5$ is a non-radiative energy transfer that was mostly attributable to electric multipolar interactions in S_{1-x}ZSO:xEu phosphors. According to Dexter's theory, luminescence intensity and activator are related, as shown by the Eq. (11) [32].

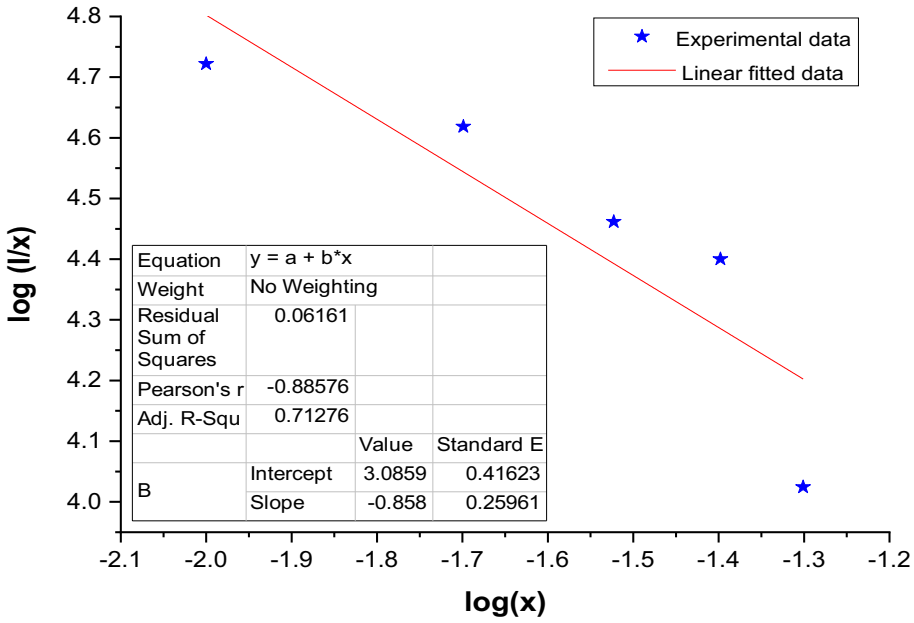

Fig. 13 The relationship between log (I/x) versus log (x) for the transition of $^5D_0 \rightarrow {}^7F_2$ (617 nm)

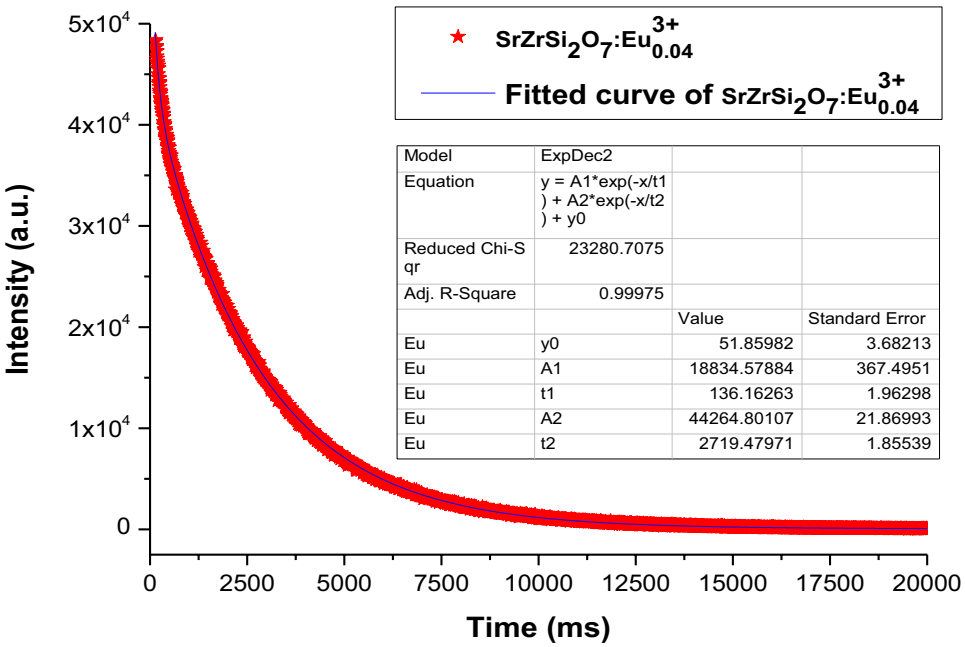

Fig. 14 Decay curves of SZSO:Eu0.04 phosphor

$$\frac{I}{x} = K\left[1 + \beta(x)^{\theta/3}\right]^{-1} \quad (11)$$

where x represents the concentration of dopant, θ is a multipolar interaction constant there are nearest neighbor ions numbers 6, 8, and 10, which mean dipole–dipole (d–d), dipole–quadrupole (d–q), and quadrupole–quadrupole (q–q) interaction respectively and K and β are constant for each interaction at the same excitation. Figure 13 shows the graph between Log (I/*x*) versus Log(x). The fitted line's slope was determined to be -0.858; thus, the calculated value is 5.17, which is close to 6. Therefore, d–d interaction could be attributed quenching effect in S_{1-x}ZSO:*x*Eu phosphors.

3.7 Decay

The effect of SZSO:Eu0.04 content on the $^5D_0 \rightarrow {}^7F_2$ transition decay curve is shown in Fig. 14. As Eu^{3+} ions at different sites were excited at the same time, the decay curve cannot be fit by a single exponential equation so it is fits well with a two-exponential equation [44]. The corresponding decay curve can be well fitted with a double exponential function, described by the **Eq.** (12)

$$Y = Y_0 + A_1 \exp\left(-\frac{x}{t_1}\right) + A_2 \exp\left(-\frac{x}{t_2}\right) \quad (12)$$

Here Y and Y_0 are luminescence intensity at time t and 0, A_1 and A_2 are constant and fast decay, and slow decay is described by t_1 and t_2 in the 0.04Eu single doped SZSO sample. The lifetime decay for an exponential component using these parameters, the fitting result of the sample is listed in Table 7. Using Eq. (12), we obtain $\tau_1 =$ 136.16263 ms and $\tau_2 =$ 2719.47971 ms which is responsible for shallow and deep trap.

The average decay time (τ_{av}) can be determined using the Eq. (13) which is given below[34].

$$\tau_{av} = \frac{A_1 {\tau_1}^2 + A_2 {\tau_2}^2}{A_1 \tau_1 + A_2 \tau_2} \quad (13)$$

On the basis of the above Eq. (13), the average luminescence decay time is determined to be 2665.59187 ms for SZSO:Eu0.04 phosphor.

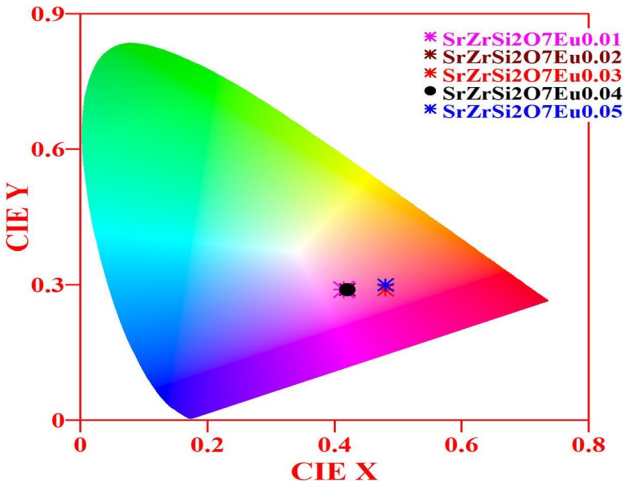

Fig. 15 CIE chromaticity diagram of S_{1-x}ZSO:xEu phosphors

3.8 Photometric properties

3.8.1 CIE chromaticity coordinate

The 1931 CIE chromatic color coordinate usually refers to the color in lighting specifications, recognizing that humans see three primary colors: red, blue, and green [31]. The chromaticity coordinates of the S_{1-x}ZSO:*x*Eu phosphor is calculated from PL spectra. A region of orange-red light, the color coordinate of the prepared sample, appears on the CIE chromaticity coordinates [45]. Figure 15 represents the CIE 1931 chromaticity diagram of S_{1-x}ZSO:xEu phosphor. The number from 0.01 to 0.05 mol presents the concentration of Eu^{3+}; and their chromaticity coordinates are (0.4140, 0.2893), (0.4171, 0.2890), (0.4795, 0.2945), (0.4168, 0.2858) and (0.4793, 0.2980) respectively.

A region of orange-red light, the color coordinate of the prepared sample, appears on the CIE chromaticity coordinates. Luminescence colors of S_{1-x}ZSO:xEu phosphors represented by the symbols [*]. Based on the Eq. (14), the color purity (CP) of all samples is calculated [45].

$$\text{Color purity} = \frac{\sqrt{(x - x_i)^2 + (y - y_i)^2}}{\sqrt{(x_d - x_i)^2 + (y_d - y_i)^2}} .100\% \quad (14)$$

These coordinates correspond with the CIE coordinates of the sample point (x, y), standard source (x_i, y_i), and dominant wavelength (x_d, y_d). The (x_i, y_i) is taken (0.33, 0.33) for standard white light [46]. The variation of percentage in CP

Table 7 Fitting results of the SZSO:0.04Eu phosphor

Sample Name	R^2_Value	τ_1 (ms)	τ_2 (ms)	A_1	A_2	τ_{avg} (ms)
SZSO:0.04Eu	0.99975	136.16263	2719.47971	18834.57884	44264.80107	2665.59187

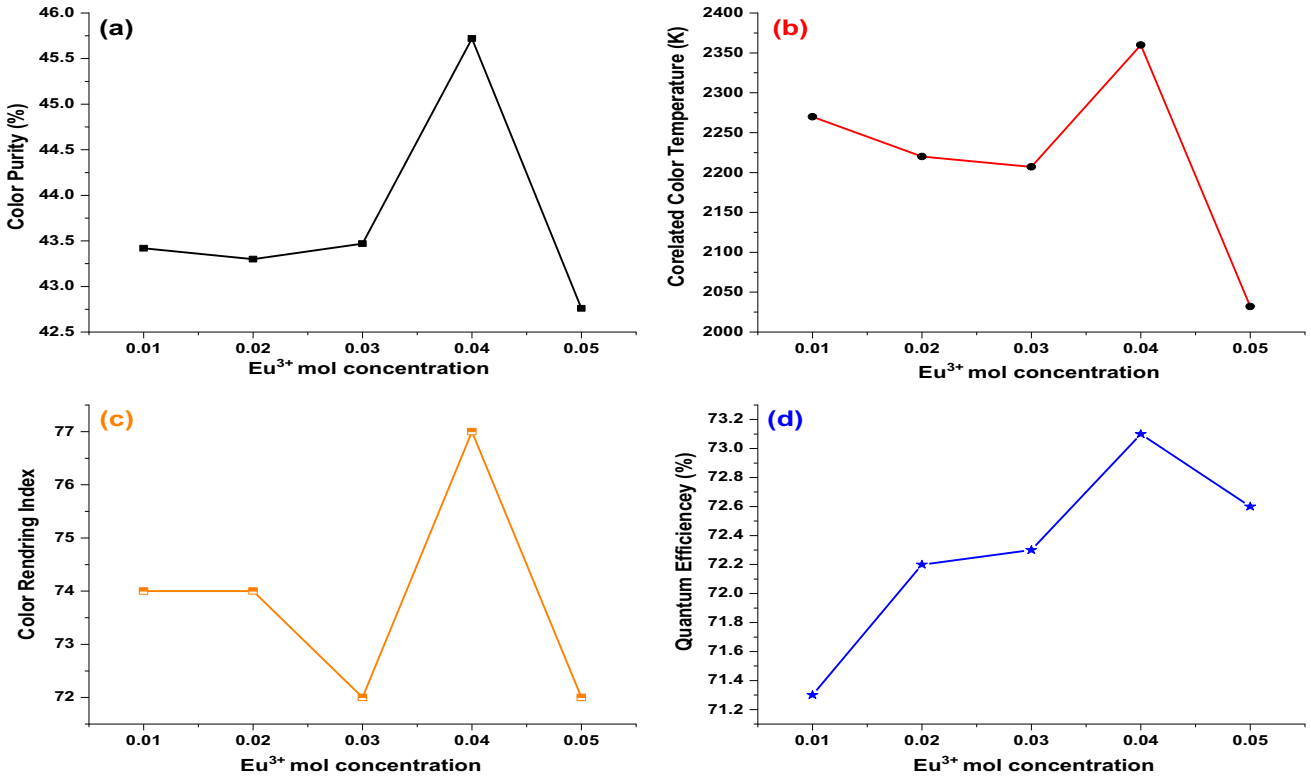

Fig. 16 **a** Variation in color purity with respect to S_{1-x}ZSO:xEu phosphors. **b** Variation in correlated color temperature with respect to S_{1-x}ZSO:xEu phosphors. **c** Variation in color rendering index with respect to S_{1-x}ZSO:xEu phosphors. **d** Variation in Quantum Efficiency with respect to S_{1-x}ZSO:xEu phosphors

Table 8 Photometric parameters of S_{1-x}ZSO:xEu phosphors

S. on	Sample code	CIE color co-ordinate (X, Y)	Dominant CIE color co-ordinate (X_d, Y_d)	Color purity (%)	CRI	CCT (K)
1	SZSO:0.01Eu	(0.4140, 0.2893)	(0.571, 0.189)	43.42	74	2270
2	SZSO:0.02Eu	(0.4171, 0.2890)	(0.572, 0.188)	43.30	74	2220
3	SZSO:0.03Eu	(0.4795, 0.2945)	(0.671, 0.237)	43.47	72	2207
4	SZSO:0.04Eu	(0.4168, 0.2858)	(0.568, 0.187)	45.72	77	2360
5	SZSO:0.05Eu	(0.4793, 0.2980)	(0.675, 0.236)	42.76	72	2032

with increasing Eu^{3+} ion concentration is displayed in Fig. 16a. The calculated CP values of prepared S_{1-x}ZSO:xEu phosphors are also listed in Table 8. It is seen that the CP values lies in between 42.76 and 45.72; it is noted that the low CP values signifies the emission of color near white region. Thus, the above outcome specify that the prepared phosphors emit orange–red color will be a potential candidate for the solid-state lighting and other display applications.

3.8.2 Correlated color temperature (CCT)

According to the literature, CCT is essentially a characteristic indicating how yellow or blue the light output by a light bulb appears [47]. It is measured in the between 2200 and 6500 Kelvin degrees. Cooler color temperatures range from 3500 to 5000 K+, whereas warmer color temperatures are between 2200 and 3000 K, featuring more light in the red, orange and yellow range [48]. The CCT values are calculated by using McCamy's approximation (Eq. (15)) [49].

$$CCT = -449n^3 + 3525n^2 - 6823.3n + 5520.33 \quad (15)$$

Table 9 Calculated Values of the absorption rate, quantum efficiency (with internal and external) of S_{1-x}ZSO:xEu phosphors

s. no.	Sample code	AR	EQE (%)	IQE (%)	QE (%)
1	SZSO:0.01Eu	67.1	50.4	62.1	71.3
2	SZSO:0.02Eu	67.4	50.6	62.3	72.2
3	SZSO:0.03Eu	67.0	50.9	61.6	72.3
4	SZSO:0.04Eu	67.9	51.1	62.5	73.1
5	SZSO:0.05Eu	67.5	50.7	62.4	72.6

where $n = x - 0.332/y - 0.186$ and (x, y) are CIE coordinates, S_{1-x}ZSO:xEu phosphor samples are listed in Table 8. The calculated CCT values lies within a range from 2207 to 2360 K in the warm region of visible for different doping concentrations of Eu^{3+} ion. The variation of CCT with increasing Eu^{3+} ion concentration is displayed in Fig. 16b. It was observed that the CCT value decreases with rising, dopant concentration. It means prepared phosphors emits light in the warm region for higher dopant concentration, whereas cool in lower concentrations [50].

3.8.3 Color rendering index (CRI)

The CRI is calculated for the significance of the light source (orange-red), it is an important parameter that describes the quality of the spectrum [51]. The values of ranges from scale of 0 to 100. CRIs in the range of 75–100 is considered excellent, while 65–75 is good. The range of 55–65 is fair, and 0–55 is poor. By using Eq. 16, the CRI values are calculated and all values is tabulated in Table 8 [37].

$$CRI = \frac{1}{8}\sum_{i=1}^{8} R_i \tag{16}$$

The calculated CRI values of prepped S_{1-x}ZSO:*x*Eu phosphors are varies from 72 to 77, showing in excellent and good range. In addition, the variation of CCT with increasing Eu^{3+} ion concentration is displayed in Fig. 16c and CRI value depends upon the concentration of Eu^{3+}. The CRI shows the maximum for the 0.04 mol Eu^{3+} concentration which is a good agreement with the result of PL emission spectrum.

3.8.4 Quantum efficiency (Q.E.) analysis

The QE of prepared S_{1-x}ZSO:*x*Eu phosphors has been calculated using Eq. (17) through the conventional methods using a standard material.

$$Q.E = \frac{I_{Sam.}}{E_{ref.} - E_{Sam.}} \tag{17}$$

where, $I_{sam.}$ = PL intensity of emission spectra of the samples, E_{sam} = PL intensity of excitation spectra of samples, $E_{ref.}$ = PL intensity of excitation spectra of reference. The internal (IQE) and external quantum efficiency (EQE) [52] was also calculated using Eqs. (18) and (19) for synthesized S_{1-x}ZSO:*x*Eu phosphors.

$$\text{Internal quantum efficiency (IQE)} = \frac{\gamma_{ab}}{\gamma_{ex} - \gamma_r} \tag{18}$$

$$\text{External quantum efficiency (EQE)} = \frac{\gamma_{ab}}{\gamma_{ex}} \tag{19}$$

where, γ_{ab} = total number of photons absorbed by sample, γ_{ex} = total number of photons emitted by the excitation, and γ_r = total number of photons reflected and not absorbed by the phosphor.

The QE, IQE, EQE and absorption rate (AR) were calculated for the sintered S_{1-x}ZSO:*x*Eu phosphors and listed in Table 9 and it is shown that, the IQE is always larger than the EQE. The calculated QE values of prepped S_{1-x}ZSO:xEu phosphors were estimated under 396 nm excitation are varies from 71.3% to 73.1% and optimum for SZSO:0.04Eu phosphor which is 73.1%. Here, SZSO:0.04Eu has found optimise and efficient sample with respect to other samples which has given excellent result. The variation of QE with increasing Eu^{3+} ion concentration is displayed in Fig. 16d and value of QE depends upon the concentration of Eu^{3+} ions.

4 Conclusion

In summary, a series of S_{1-x}ZSO:*x*Eu phosphors were synthesized by a high- temperature solid-state reaction method. It is found that the Eu^{3+} ions successfully incorporated on Sr^{2+} ions lattice site of SZSO host. The luminescence studies of phosphor exhibited strong absorption near UV light under the excitation of 396 nm. The phosphor indicates two strong emission peaks at 595 nm ($^5D_0 \rightarrow {}^7F_1$) and 617 nm ($^5D_0 \rightarrow {}^7F_2$) where electric dipole transition (EDT) $^5D_0 \rightarrow {}^7F_2$ is hypersensitive which is favored in red color emission. The optimum luminescence properties are obtained at a 0.04 mol doping concentration of Eu^{3+} ions in the SZSO host. After then concentration quenching obtains proved owing due to the energy transfer between nearest-neighbor ions. The average luminescence decay time is determined 2665.59187 ms for optimized phosphor due to florescent persistence luminescence phenomenon. The photometric studies are well within the defined acceptable range indicate that prepared phosphor emitted orange-red light and useful for the solid-state lighting applications.

Acknowledgements The corresponding author; Dr. Ishwar Prasad Sahu, would like to acknowledge the Science & Engineering Research Board (SERB), New Delhi, Government of India for funding FTIR

Spectrophotometer (CRG/2018/004139). This instrument is used for the IR spectroscopic analysis of the prepared sample from the study.

Author contributions Ishwar Prasad Sahu and Manorama Sahu: Investigate, designed the whole research, Conceptualization, synthesized all the samples, and collected experimental data, Data plotting, writing of the manuscript, review, editing and formatting, and editing of manuscript corresponding to the journals.

Funding This work was supported by UGC-BSR Start-up Fellowship: No. F.30–420/2018 (BSR), dated 23/10/2018, the Corresponding Author Dr. Ishwar Prasad Sahu, has received research support from University Grant commission (UGC), New Delhi, Government of India.

Data availability The author's states that analysed and relevant data of synthesized materials, which are including and described in the manuscript will be freely available to researchers and scientists who are working purpose of research and social welfare.

Declarations

Conflict of interest On behalf of all authors, the corresponding author states that there is no conflict of interest.

Ethical approval This is an experimental study on materials science and no ethical approval is required.

References

1. H. Guo, Q. Shi, K.V. Ivanovskikh, L. Wang, C. Cui, P. Huang, A high color purity red-emission phosphor based on Sm^{3+} and Eu^{3+} co-doped $Ba_3Bi(PO_4)_3$. Mater. Res. Bull. **126**, 110836 (2020). https://doi.org/10.1016/j.materresbull.2020.110836
2. B. Yu, Y. Li, R. Zhang, H. Li, Y. Wang, A novel thermally stable eulytite-type $NaBaBi_2(PO_4)_3$:Eu^{3+} red-emitting phosphor for pc-WLEDs. J. Alloys Compd. **852**, 157020 (2021). https://doi.org/10.1016/j.jallcom.2020.157020
3. Y. Peng, Q. Sun, J. Liu, H. Cheng, Y. Mou, Fabrication of stacked color converter for high-power WLEDs with ultra-high color rendering. J. Alloys Compd. **850**, 156811 (2021). https://doi.org/10.1016/j.jallcom.2020.156811
4. Y. Gao, Y. Li, X. Sun, P. Jiang, R. Cong, T. Yang, Dopant and excitation wavelength dependent color tunability in Dy^{3+} and Eu^{3+} doped $CaBi_2B_2O_7$ phosphors for NUV warm white LEDs. Mater. Res. Bull. **122**, 110649 (2020). https://doi.org/10.1016/j.materresbull.2019.110649
5. M. Qu, X. Zhang, X. Mi, H. Sun, Q. Liu, Z. Bai, Luminescence color tuning of Ce^{3+} and Tb^{3+} co-doped $Ca_2YZr_2Al_3O_{12}$ phosphors with high color rendering index via energy transfer. J. Lumin. **228**, 117557 (2020). https://doi.org/10.1016/j.jlumin.2020.117557
6. T. Takeda, K. Kato, H. Kiyono, N. Hirosaki, Powder synthesis and luminescence properties of green emitting $Ba_2LiSi_{7-x}Al_xN_{12-x}O_x$:$Eu^{2+}$ phosphor. J. Alloys Compd. **850**, 156358 (2021). https://doi.org/10.1016/j.jallcom.2020.156358
7. V.R. Bandi, M. Jayasimhadri, J. Jeong, K. Jang, H.S. Lee, S.S. Yi, J.H. Jeong, Host sensitized novel red phosphor $CaZrSi_2O_7$:Eu^{3+} for near UV and blue led-based white LEDs. J. Phys. D Appl. Phys. **43**, 395103 (2010). https://doi.org/10.1088/0022-3727/43/39/395103
8. Z. Zhou, G. Liu, J. Ni, W. Liu, Q. Liu, Simultaneous multi-wavelength ultraviolet excited single-phase white light emitting phosphor Ba_{1-x}(Zr, Ti)S_i3_O9:xEu. Opt. Mater. **79**, 53–62 (2018). https://doi.org/10.1016/j.optmat.2018.03.018
9. P. Feng, J. Zhang, C. Wu, Z. Liu, Y. Wang, Self-activated afterglow luminescence of un-doped $Ca_2ZrSi_4O_{12}$ material and explorations of new afterglow phosphors in a rare earth element-doped $Ca_2ZrSi_4O_{12}$ system. Mater. Chem. Phys. **141**(1), 495–501 (2013). https://doi.org/10.1016/j.matchemphys.2013.05.049
10. M.E. Huntelaar, E.H.P. Cordfunke, P.V. Vlaanderen, $SrZrSi_2O_7$. Acta Cryst. C **50**, 988 (1994). https://doi.org/10.1107/S0108270193008364
11. G. Blasse, W.J. Schipper, M.E. Huntelaar, D.J.W. Ijdo, Luminescence of $SrZrSi_2O_7$. J. Phys. Chem. Solids **54**(9), 1001–1003 (1993). https://doi.org/10.1016/0022-3697(93)90004-B
12. I. Ahemen, F.B. Dejene, R.E. Kroon, H.C. Swart, Effect of europium ion concentration on the structural and photoluminescence properties of novel Li_2BaZrO_4:Eu^{3+}nanocrystals. Opt. Mater. **74**, 58–66 (2017). https://doi.org/10.1016/j.optmat.2017.03.029
13. D.V. Deyneko, I.V. Nikiforov, B.I. Lazoryak, D.K. Spassky, I.I. Leonidov, S.Y. Stefanovich, D.A. Petrova, S.M. Aksenov, P.C. Burns, $Ca_8MgSm_{1-x}(PO_4)_7$:xEu^{3+}, promising red phosphors for WLED application. J. Alloys Compd. **776**, 897–903 (2019). https://doi.org/10.1016/j.jallcom.2018.10.317
14. X. Lu, H. Liu, X. Yang, Y. Tian, X. Gao, L. Han, Q. Xu, A single-phase white-emitting $La_{10}(SiO_4)_6O_3$:Eu^{2+} /Eu^{3+} phosphor for near-UV LED-based application. Ceram. Int. **43**(15), 11686–11691 (2017). https://doi.org/10.1016/j.ceramint.2017.05.358
15. Y. Yuan, H. Lin, J. Cao, Q. Guo, F. Xu, L. Liao, L. Mei, A novel blue-purple Ce^{3+} doped whitlockite phosphor: synthesis, crystal structure, and photoluminescence properties. J. Rare Earths **39**(6), 621–626 (2021). https://doi.org/10.1016/j.jre.2020.07.013
16. S. Kaur, M. Jayasimhadri, A.S. Rao, A novel red emitting Eu^{3+} doped calcium aluminozincate phosphor for applications in w-LEDs. J. Alloys Compd. **697**, 367–373 (2017). https://doi.org/10.1016/j.jallcom.2016.12.150
17. J.D. Xiaopyan, X. Pan, Z. Liu, Y. Jing, B. Wang, L. Luo, J. Wang, P. Du, Highly efficient Eu^{3+}-activated $Ca_2Gd_8Si_6O_{26}$ red-emitting phosphors: a bifunctional platform towards white light-emitting diode and ratio metric optical thermometer applications. J. Alloys Compd. **859**, 157843 (2021). https://doi.org/10.1016/j.jallcom.2020.157843
18. B. Fan, J. Liu, W. Zhao, L. Han, Luminescence properties of Sm^{3+} and Dy^{3+} co-doped BaY_2ZnO_5 phosphor for white LED. J. Lumin. **219**, 116887 (2020). https://doi.org/10.1016/j.jlumin.2019.116887
19. G.L. Bhagyalekshmi, D.N. Rajendran, Luminescence dynamics of Eu^{3+} activated and co-activated defect spinel zinc titanate nanophosphor for applications in WLEDs. J. Alloys Compd. **850**, 156660 (2021). https://doi.org/10.1016/j.jallcom.2020.156660
20. H. Duan, R. Cui, J. Li, C. Deng, Synthesis and photoluminescence properties of a novel red emitting $Ba_3ZnTa_2O_9$: Eu^{3+} phosphor. J. Mol. Struct. **1224**, 129075 (2021). https://doi.org/10.1016/j.molstruc.2020.129075
21. D. Lundberg, D. Warmińska, A. Fuchs, I. Persson, On the relationship between the structural and volumetric properties of solvated metal ions in *O*-donor solvents using new structural data in amide solvents. Phys. Chem. Chem. Phys. **20**(21), 14525 (2018). https://doi.org/10.1039/c8cp02244e
22. C. Lorbeer, F. Behrends, J. Cybinska, H. Eckertbd, A.V. Mudring, Charge compensation in RE^{3+} (RE = Eu, Gd) and M^+ (M = Li, Na, K) co-doped alkaline earth nanofluorides obtained by microwave reaction with reactive ionic liquids leading to improved optical properties. J. Mater. Chem. C **2**, 9439 (2014). https://doi.org/10.1039/c4tc01214c
23. M. Peng, Z. Pei, G. Hong, Q. Su, The reduction of Eu^{3+} to Eu^{2+} in $BaMgSiO_4$: Eu prepared in air and the luminescence of

$BaMgSiO_4:Eu^{2+}$ phosphor. J. Mater. Chem. **13**, 1202 (2003). https://doi.org/10.1039/B211624C
24. Y. Ma, S. Chen, J. Che, J. Wang, R. Kang, J. Zhao, B. Deng, R. Yu, H. Geng, Effect of charge compensators (Li^+, Na^+, K^+) on the luminescence properties of $Sr_3TeO_6:Eu^{3+}$ red phosphor. Ceram. Int. **47**(6), 8518–8527 (2021). https://doi.org/10.1016/j.ceramint.2020.11.219
25. X. Li, Z. Zou, Z. Wang, C. Wu, J. Znang, Y. Wang, A novel undoped long lasting phosphorescence phosphor: SrZrSi2O7. J. Rare Earths **33**(1), 37–41 (2015). https://doi.org/10.1016/S1002-0721(14)60380-X
26. H. Guo, X. Huang, Low-temperature solid-state synthesis and photoluminescence properties of novel high-brightness and thermal-stable Eu^{3+}-activated $Na_2Lu(MoO_4)(PO_4)$ red-emitting phosphors for near-UV-excited white LEDs. J. Alloys Compd. **764**, 809–814 (2018). https://doi.org/10.1016/j.jallcom.2018.06.156
27. R. Nagaraj, A. Raja, S. Ranjith, Synthesis and luminescence properties of novel red-emitting Eu^{3+} ions doped silicate phosphors for photonic applications. J. Alloys Compd. **827**, 154289 (2020). https://doi.org/10.1016/j.jallcom.2020.154289
28. X. Meng, S. Huang, M. Shang, Red emitting $Ba_2GdVO_6:Eu^{3+}$ phosphors for blue light converted warm white LEDs. Inorg. Chem. Commun. **113**, 107768 (2020). https://doi.org/10.1016/j.inoche.2020.107768
29. R.D. Shannon, Revised effective ionic radii and systematic studis of interatomic distances in halides and chalcogenides. Acta Cryst. **A32**, 751–767 (1976). https://doi.org/10.1107/S0567739476001551
30. G.V. Kanmani, V. Ponnusamy, G. Rajkumar, M.T. Jose, Development of novel $Na_2Mg_3Zn_2Si_{12}O_{30}:Eu^{3+}$ red phosphor for white light emitting diodes. Opt. Mater. **96**, 109350 (2019). https://doi.org/10.1016/j.optmat.2019.109350
31. S. Ray, P. Tadge, S. Dutta, T.M. Chen, G.B. Nair, S.J. Dhoble, Synthesis, luminescence and application of $BaKYSi_2O_7:Eu^{2+}$: a new blue-emitting phosphor for near-UV white-light LED. Ceram. Int. **44**(7), 8334–8343 (2018). https://doi.org/10.1016/j.ceramint.2018.02.022
32. R. Cao, Y. Ren, T. Chen, W. Wang, Q. Guo, Q. Hu, C. Liao, T. Fan, Emission improvement and tunable emission properties of $SrZrSi_2O_7$: R ($R = S^{m3}$+and S^{m3}+ /B^{i3}+) phosphors. J. Lumin. **225**, 117350 (2020). https://doi.org/10.1016/j.jlumin.2020.117350
33. S.J. Park, J.Y. Kim, J.H. Yim, N.Y. Kim, C.H. Lee, S.J. Yang, H.K. Yang, The effective fingerprint detection application using $Gd_2Ti_2O_7:Eu^{3+}$ nanophosphors. J. Alloys Compd.. **741**, 246–255 (2018). https://doi.org/10.1016/j.jallcom.2018.01.116
34. Golja DR, Dejene FB (2020) Effect of Eu^{3+} ion concentration on the structural and photoluminescence properties of $Ba_{1.3}Ca_{0.7}SiO_4$ ceramic-based red phosphors for solid- state lighting applications. J. Alloys Compd. 827: 154216. https://doi.org/10.1016/j.jallcom.2020.154216
35. C. Manjunath, M.S. Rudresha, R. HariKrishna, B.M. Nagabhushana, B.M. Walsh, K.R. Nagabhushana, B.S. Panigrahi, Spectroscopic studies of strong red emitting $Sr_2SiO_4:Eu^{3+}$ nanophosphors with high color purity for application in WLED using Judd-Ofelt theory and TL glow curve analysis. Opt. Mater. **85**, 363–372 (2018). https://doi.org/10.1016/j.optmat.2018.08.070
36. X. Huang, Q. Sun, B. Devakumar, Preparation, crystal structure, and photoluminescence properties of high-brightness red-emitting $Ca_2LuNbO_6:Eu^{3+}$ double- perovskite phosphors for high-CRI warm-white LEDs. J. Lumin. **225**, 117373 (2020). https://doi.org/10.1016/j.jlumin.2020.117373
37. S. Som, A.K. Kunti, V. Kumar, V. Kumar, S. Dutta, M. Chowdhury, S.K. Sharma, J.J. Terblans, H.C. Swart, Defect correlated fluorescent quenching and electron phonon coupling in the spectral transition of Eu^{3+} in $CaTiO_3$ for red emission in display application. J. Appl. Phys. **115**(19), 1–14 (2014). https://doi.org/10.1063/1.4876316
38. S.K. Sharma, S. Som, R. Jain, A.K. Kunti, Spectral and CIE parameters of red emitting $Gd_3Ga_5O_{12}:Eu^{3+}$ phosphor. J. Lumin. **159**, 317–324 (2015). https://doi.org/10.1016/j.jlumin.2014.11.010
39. P. Aryal, H.J. Kim, A. Khan, S. Saha, S.J. Kang, S. Kothan, Y. Yamsuk, J. Kaewkhao, Development of Eu^{3+}-doped phosphate glass for red luminescent solid- state optical devices. J. Lumin. **227**, 117564 (2020). https://doi.org/10.1016/j.jlumin.2020.117564
40. Q. Wu, Y. Xie, F. She, Q. Zhao, J. Ding, J. Zhou, $CsBaB_3O_6:Eu^{3+}$ red-emitting phosphors for white LED and FED: Crystal structure, electronic structure and luminescent properties. J. Rare Earths **39**(9), 1040–1048 (2021). https://doi.org/10.1016/j.jre.2020.07.014
41. K. Mondal, D.K. Singh, J. Manam, Spectroscopic behavior, thermal stability and temperature sensitivity of Ca_2SiO_4: Eu^{3+} red emitting phosphor for solid state lighting application. J. Alloys Compd. **761**, 41–51 (2018). https://doi.org/10.1016/j.jallcom.2018.05.161
42. Z. Zhang, L. Sun, B. Devakumar, G. Annadurai, J. Liang, S. Wang, Q. Sun, X. Huang, Synthesis and photoluminescence properties of a new blue-light- excitable red phosphor $Ca_2LaTaO_6:Eu^{3+}$ for white LEDs. J. Lumin. **222**, 117173 (2020). https://doi.org/10.1016/j.jlumin.2020.117173
43. K.K. Rasu, S.M. Babu, Impact of Eu3+ concentration on the fluorescence properties of the $LiGd(W_{0.5}Mo_{0.5}O_4)2$ novel red phosphors. Solid State Sci. **98**, 106028 (2019). https://doi.org/10.1016/j.solidstatesciences.2019.106028
44. T. Sakthivel, G. Annadurai, R. Vijayakumar, X. Huang, Synthesis, luminescence properties and thermal stability of Eu^{3+}-activated $Na_2Y_2B_2O_7$ red phosphors excited by near-UV light for pc-WLEDs. J. Lumin. **205**, 129–135 (2019). https://doi.org/10.1016/j.jlumin.2018.09.008
45. G. Blasse, Energy transfer in oxidic phosphors. Phys. Lett. A **28**(6), 444–445 (1968). https://doi.org/10.1016/0375-9601(68)90486-6
46. D.L. Dexter, A theory of sensitized luminescence in solids. J. Chem. Phys. **21**(5), 836–850 (1953). https://doi.org/10.1063/1.1699044
47. L. Zhang, Y. Xie, X. Geng, B. Deng, H. Geng, R. Yu, Double perovskite $Ca_2MgTeO_6:Eu^{3+}$ red-emitting phosphors with high thermal stability for near UV/blue excited white LEDs. J. Lumin. **225**, 117365 (2020). https://doi.org/10.1016/j.jlumin.2020.117365
48. S.K. Baghel, N. Brahme, D.P. Bisen, Y. Patle, T. Richhariya, E. Chandrawanshi, C. Belodhiya, Luminescence properties of a novel cyan-blue light emitting Ce^{3+}doped $SrZrSi_2O_7$ phosphor. Opt. Mater. **126**, 112141 (2022). https://doi.org/10.1016/j.optmat.2022.112141
49. C.S. McCamy, Correlated color temperature as an explicit function of chromaticity coordinates. Color. Res. Appl. **17**(2), 142–144 (1992). https://doi.org/10.1002/col.5080170211
50. Y. Zhong, P. Sun, X. Gao, Q. Liu, S. Huang, B. Liu, B. Deng, R. Yu, Synthesis and optical properties of new red-emitting SrBi2Ta2O9:Eu3+ phosphor application for w-LEDs commercially based on InGaN. J. Lumin. **212**, 45–51 (2019). https://doi.org/10.1016/j.jlumin.2019.03.057
51. J. Xue, H.M. Noh, S.H. Park, B.C. Choi, J.H. Kim, J.H. Jeong, P. Du, W. Ran, M. Song, Eu3+-activated $Ca_3Mo_{0.2}W_{0.8}O_6$ red-emitting phosphors: a near-ultraviolet and blue light excitable platform for solid-state lighting and thermometer. J. Lumin. **223**, 117212 (2020). https://doi.org/10.1016/j.jlumin.2020.117212
52. R.K. Singh, S. Som, C.H. Lu, Spectroscopic investigation of red Eu^{3+} doped ceria nanophosphors and promising color rendition for warm white LEDs. J. Alloys Compd. **816**, 152653 (2020). https://doi.org/10.1016/j.jallcom.2019.152653